DETECTION AND CHARACTERIZATION OF THE TUMOR CHANGE BETWEEN TWO FDG PET SCANS USING PARAMETRIC IMAGING

H. Necib, M. Dusart, B. Vanderlinden, I. Buvat.

IMNC - U8165 CNRS – Paris 7 – Paris 11, Orsay, France, Dosisoft, Cachan, France, Institut Jules Bordet, Bruxelles, Belgique.
necib@imnc.in2p3.fr, michelle.dusart@bordet.be, bruno.vanderlinden@bordet.be, buvat@imnc.in2p3.fr

ABSTRACT

Patient follow-up based on PET scans is a promising approach for early assessment of tumor response and for detection of tumor recurrence. In this work, we introduce a parametric imaging method to detect and analyze the tumor changes between 2 consecutive PET scans. Fifteen pairs of consecutives PET/CT images obtained during the course of lung cancer patient monitoring were considered. For each pair, after CT-based registration of the PET images, the two PET datasets were subtracted. A biparametric graph of subtracted voxel values versus voxel values in the first scan was obtained. A model-based analysis of this graph was used to identify the tumor voxels in which significant changes occurred between the 2 scans, and yielded indices characterizing the changes. In our patients, the proposed approach correctly identified all tumor changes as confirmed using a conventional analysis. In addition, the parametric imaging approach can reveal heterogeneities in tumor response and does not require the preliminary identification of the tumors.

Index Terms— Positron emission tomography, Tumors, Registration, Biomedical monitoring

1. INTRODUCTION

Positron Emission Tomography (PET) might play a major role in patient monitoring in a near future [1]. Indeed, this functional imaging modality makes it possible to detect early changes in metabolic activity of the tumor, before these changes introduce anatomical abnormalities that can be seen using conventional anatomical imaging modalities [2].

Tumor changes occurring between PET scans acquired before and during the course of therapy are most often assessed visually. Indices characterizing the tumor uptake, such as the Standardized Uptake Values (SUV) [3] are also reported. This requires the identification of each tumor, so that the SUV corresponding to each tumor can then be calculated. Recommendations about how to interpret SUV changes between scans have been published [4] and are based on using thresholds in SUV changes to classify tumor change. For instance, a decrease in SUV greater than 25% associated with a decrease in tumor volume as assessed visually is interpreted as a partial metabolic response. These recommendations have many limitations however [5], given the large variability in SUV and volume estimation methods [6]. In addition, in this approach, the tumor is considered as a whole, without considering possible differences in behavior within the tumor, such the presence of a necrotic or semi-necrotic regions.

The objective of this study was to propose a parametric imaging method to assess tumor changes at the voxel level, without averaging over pre-defined tumor regions. By retaining information at the voxel level, such an approach might give evidence, if any, of heterogeneous behavior within a tumor. In addition, parametric imaging does not require a preliminary identification of the tumors: all regions (related to the tumor(s) or not) in which activity has significantly changed between the two scans are first identified. The parametric images are then further analyzed to distinguish changes related to tumor growth or tumor response from other physiological changes.

2. MATERIALS AND METHODS

2.1. Data acquisition

The method was developed based on clinical cases, to make sure our models accounted for all the complexity of real data.
Two lung cancer patients were considered, with eight tumors in total. One patient underwent 3 Fluorine-18-fluorodeoxyglucose (FDG) PET/CT scan, one prior to any therapy, the second 12 weeks after the beginning of chemotherapy (3 cycles) and the third 11 weeks after (3 cycles). The second patient underwent 5 PET/CT scans, one prior to any therapy, the second 12 weeks after the beginning of therapy (2 cycles), then 11 weeks after (4 cycles), then 12 weeks after (3 cycles), and finally 11 weeks after (no cycles).

FDG PET/CT images were obtained on a GE Discovery LS system 60 min post-injection of 4 MBq/kg. Images were reconstructed using the ordered subset expectation maximization algorithm [7] with 2 iterations and 28 subsets and post-smoothed with a 5.45 mm FWHM Gaussian filter. Attenuation was compensated for using the CT data and scatter was corrected for using a convolution subtraction. In each PET/CT scan, the PET (4.25 mm slice thickness, 128x128 pixels of 3.91 mm x 3.91 mm) and CT (5 mm slice thickness, 512x512 pixels of 0.98 mm x 0.98 mm) images were co-registered.
To compare PET scans acquired before and over the course of therapy, the images were converted in SUV units, by normalizing the observed activity by the injected activity per body weight corrected for radioactive decay.

2.2. Registration of consecutive PET scans

To compare two consecutive PET scans at a voxel level, these scans are first registered so that a given voxel always corresponds to the same volume element in the patient. Because PET and CT scans acquired during the same imaging session are already registered, the CT data associated with each PET scan are used to realign the PET scans [8]. Indeed, the CT data include more landmarks than the PET data to guide the registration algorithm. The CT/CT registration is performed by considering a rigid transform (3 translation and 3 rotation parameters), which is optimized using a least mean square criterion within a large volume of interest (Pixies^{TM} software). The CT/CT transformation matrix is then applied to the PET data. The second scan (in time) is always realigned to match the first scan. Only a small set of relevant slices given the tumor location(s) is registered. A preliminary investigation based on consistency measurements [9, 10, 11] was performed to assess the

performance of our registration approach in our context.

2.3. Parametric imaging

The 2 registered PET scans are first subtracted voxel-by-voxel. The resulting dataset is then analyzed using a biparametric approach. This analysis identifies the tumor regions in the subtracted dataset. A parametric 3D image displaying only voxels related to tumor changes is finally obtained.

2.3.1. Subtraction datasets and biparametric graphs

The 2 registered PET datasets PET1 and PET2 are first subtracted voxel by voxel: PET1(i) – PET2(i), where i denotes the voxel.

A biparametric graph of PET1(i) – PET2(i) (y axis in SUV units) versus PET1(i) (x axis in SUV units) is then obtained, with a number of points equal to the number of voxels in the analyzed dataset. In this graph, voxels that have not changed much between the two scans will be near the x axis (y close to zero), while voxels that have substantially changed will be far from the x axis (high |y| values). In addition, tumor voxels will tend to have high x values. The location of the voxels in this biparametric representation makes it possible to distinguish changes related to the tumors from changes due to noise or physiological uptakes.

2.3.2. Analysis of the biparametric graph

To distinguish tumor voxels from physiological changes in the biparametric graph, the graph is fitted using a Gaussian mixture model. Indeed, Gaussian mixture models have been shown to be useful for identifying clusters in structured data [12]. Each voxel is characterized by 2 variables corresponding to the x and y values of the biparametric graph (see section 2.3.1). The Gaussian mixture model assumes that the distribution of the voxels in this biparametric space can be expressed as a mixture of Gaussian distributions. An expectation maximization (EM) approach is used to calculate the maximum likelihood estimates of the parameters of these distributions. This results in the classification of the voxels into several classes.

Let *In* be an initial image and *Su* be the associated subtraction image, each consisting of N voxels. Let $x_i=(x_i^{In},x_i^{Su})$ be a 2-component at voxel i, where $i=1,...,N$, x_i^{In} is the initial image intensity at voxel i and x_i^{Su} is the subtraction image intensity at voxel i. The data $(x_1,...,x_N)\in\mathbf{R}^2$ are assumed to be independent and identically distributed with probability density functions :

$$\mathbf{f(x_i)=\sum_{k=1}^{K} p_k \phi(x_i|\mu_k,\Sigma_k)}$$

where K represents different evolutions of tissues in the images (P_k being the partition of the voxels), each being characterized by a Gaussian probability density function $\boldsymbol{\phi(x_i|\mu_k,\Sigma_k)}$ parameterized with a mean vector μ_k and a variance matrix Σ_k. and p_k are the mixing proportions ($0<p_k<1$ for all k=1,...,K and $\Sigma_k\, p_k=1$).

Let $c=(c_{ik},i=1,...,N;k=1,...,K)$ be a partition with $c_{ik}=1$ if $x_i\in P_k$ and 0 otherwise.

With this convention, the parameter $\theta=(p_1,...,p_{k-1},\mu_1,...,\mu_k,\Sigma_1,...,\Sigma_k)$ is chosen to maximize the log-likelihood:

$$\mathbf{L(\theta|x_1,...,x_N,c_{ik})=\sum_{i=1}^{N} ln\left[\sum_{k=1}^{K} c_{ik} p_k \phi(x_i|\mu_k,\Sigma_k)\right]}$$

Starting from an initial parameter $\theta°$ and a partition P°, an iteration of the algorithm consists in computing the current conditional probabilities $t_k(x_i)$ $(1\le i\le N; 1\le k\le K)$ for the *kth* mixture component and the current value of θ (E step):

$$\mathbf{t_k(x_i)=\frac{p_k \sum_{k=1}^{K} \phi(x_i|\mu_k,\Sigma_k)}{\sum_{m=1}^{K} \phi(x_i|\mu_m,\Sigma_m)}}$$

The M step then estimates (p_k, μ_k, Σ_k) using the cluster P_k and the conditional probability $t_k(x_i)$.

Solving the mixture model described above requires an estimate of the number of classes, an initialization of the model parameters, and a stopping criterion. Initially, 4 classes are considered: one corresponding to noise only, one including voxels in which physiological changes not related to the tumor(s) occured, one for tumor voxels responding to therapy, and one for tumor voxels corresponding to tumor progression. Simple criteria characterizing the absolute and respective positions of voxels in the biparametric graphs are used to determine how many of these classes are present in the graph.

Once the number of class C is approximately identified, a first partition of the voxels into C classes is obtained based on the absolute and relative position of the voxels in the biparametric space, but without any assumption regarding the statistical distribution of the data. This first classification is used as an initialization step for solving the Gaussian mixture model using the EM approach. A specific Gaussian mixture model is used, in which the volumes and shapes of the clusters can vary between clusters, but the orientations are identical [13], which constrains the expression of the variance matrices of the clusters. The EM algorithm is stopped when the change in the log likelihood is less than 0.001 between two successive iterations or after 150 iterations.

The EM algorithm then results in a partition of the voxels into 2, 3 or 4 classes. An analysis of this partition based on the relative size of the different clusters (tumor clusters are always supposed to be smaller than clusters corresponding to voxels affected by physiological changes only) and on the spread of the Gaussian distributions is finally performed to identify the tumor classes.

Finally, only the voxels corresponding to the tumor class(es) are shown on the PET1(i) – PET2(i) dataset. The resulting parametric 3D image thus only includes voxels in which tumor changes different from non-tumor physiological changes occurred.

2.4. Assessment of the parametric imaging method

To the best of our knowledge, no other methods for creating parametric images of tumor changes in the context of therapy monitoring have been described in the literature yet. To assess the relevance of our approach, we thus compared regional measurements made on the tumor volumes seen on our parametric images with conventional criteria that can be used to assess tumor changes.

Using our parametric images, the tumor volumes ΔV affected by changes in SUV can be easily deduced by counting the voxels corresponding to each tumor in the parametric images. Similarly, the maximum SUV change in the parametric images, ΔSUV, can be easily derived. These changes in tumor volumes and tumor SUV were compared to those obtained using conventional approaches consisting in measuring the tumor

feature in each of the 2 scans, and then subtracting the two values. For these conventional analyses, 3 tumor volume estimates were considered:

- V40: the tumor volume was calculated from the number of contiguous voxels (in the 3 dimensions) with an SUV greater than 40% of the maximum SUV in the tumor.
- VB: the tumor volume included all contiguous voxels with an intensity greater than a threshold that was a function of the maximum SUV in the tumor and of the background activity [14].
- VE: the tumor volume was manually drawn by a nuclear physician.

For the conventional analyses, tumor SUV was considered as equal to the maximum SUV in the tumor.

If the ΔV obtained from the parametric images are consistent with those obtained by subtracting the tumor volumes measured on the first and second scans, we should have:

$$|\max(V1-V2)| \leq \Delta V \leq \max(V1,V2) \quad \text{(equation 1)}$$

where max (V1-V2) denotes the maximum difference between the tumor volumes observed in scans 1 and 2 over the three volume estimates (V40, VB and VE), and max(V1,V2) denotes the maximum volumes over the 6 volume estimates (3 volume estimates for each of the two scans).

Similarly, if ΔSUV are consistent with differences in SUV measured from each scan, we should have:

$$|\Delta SUV| \geq |SUV1-SUV2| \quad \text{(equation 2)}$$

where SUV1-SUV2 is the subtraction of the maximum SUV in the tumor as seen in scan 2 from the maximum SUV in the tumor as seen in scan 1.

3. RESULTS

In total, 15 pairs of consecutive PET/CT images were compared.

3.1. PET/PET registration

The registration of each of the 15 pairs of PET datasets based on the CT registration was deemed satisfactory by visual assessment and no misregistration artifacts were seen at the edges of organs. The consistency measurements led to a mean registration error (±1 sd) of 2.9 mm ± 3.3 mm, that is, on average, less than the voxel size (3.91mm*3.91mm*4.25mm).

3.2. Parametric imaging

Figure 1 shows an example of biparametric graph describing the changes between two consecutive PET scans. Each black dot corresponds to a voxel in the analyzed volume. The figure also shows the solution of the Gaussian mixture model: voxels in the green region correspond to noise, voxels in the red region correspond to voxels in which non-tumoral physiological changes occurred between the two scans, and voxels in the blue region correspond to tumor voxels that have responded to therapy (SUV in the first scan larger than SUV in the second scan, and high SUV in the first scan).

One slice through the PET1-PET2 volume is shown in Figure 2, before (top) and after (bottom) identification of the voxels affected by tumor changes. The bottom image is what we call the parametric volume showing only regions in which tumor changes have occurred. This image was obtained from the analysis of the biparametric graph shown in Figure 1. In that case, the tumor clearly responded to therapy.

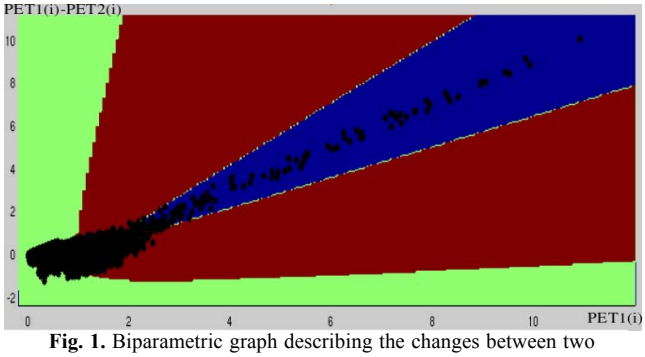

Fig. 1. Biparametric graph describing the changes between two consecutive PET scans (see comments in section 3.2).

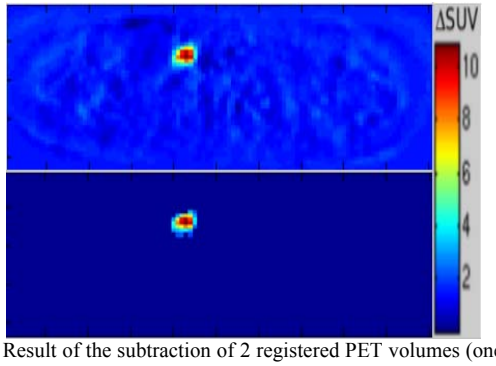

Fig. 2. Result of the subtraction of 2 registered PET volumes (one slice through the volume) and associated parametric volume after identification of the tumor region through the Gaussian mixture model analysis of the graph shown in Fig 1.

For the 15 pairs of PET scans that were compared, all tumor changes reported in the physician report (9 responses, 6 progressions) were displayed on the parametric volume. No false alarms (voxels in the parametric volume not corresponding to tumor changes) were observed in the parametric volumes.

3.3. Assessment of the parametric volumes

pairs PET scans	1	2	3	4	5	6	7	8	9	10	11	12
|ΔSUV|	16.29	6.15	14.28	13.14	3.86	10.2	12.59	10.03	12.24	3.70	5.88	3.10
|SUV1-SUV2|	6.65	1.77	5.59	4.76	1.36	7.31	4.77	1.76	7.37	2.47	2.71	1.95

Table 1. Comparison of |ΔSUV| and |SUV1-SUV2| (see equation 2) for all pairs of PET scans.

Equation 2 was verified for all 15 pairs of images (Table 1), suggesting that the maximum change in SUV deduced from the parametric volume is consistent with the difference in maximum SUV measured in each of the two scans to be compared. This does not prove that the parametric volume yields an accurate estimate of the SUV decrease or increase between the 2 scans (especially given that partial volume effect is not accounted for) but confirms that the parametric volume bears similar SUV information as the original images while retaining information at a voxel level (instead of averaging over a region or looking at one voxel value only when considering SUVmax).

pairs PET scans	1	2	3	4	5	6	7	8	9	10	11	12	13	14	15
Dv	24.69	8.71	20.53	19.95	2.86	5.52	21.05	5.65	37.56	28.78	0.85	2.97	1.36	0.65	1.17
max|V1-V2|	13.81	0.57	4.35	19.42	0.52	0.84	1.04	2.27	15.5	0.39	0.45	0.06	0.91	0.45	0.26
max(V1,V2)	29.39	9.84	14.69	46.95	8.16	7.64	18.03	10.44	46.04	23.61	2.79	2.92	2.21	2.01	15.05

Table 2. Comparison of max|(V1-V2)|, ΔV and |max(V1,V2)| (see equation 1) for all pairs of PET scans.

Equation 1 was verified for all 15 pairs of images except 3, 7 and 10 (Table 2). Looking closely at the 3 exceptions, it was found that in two cases (3 and 7 in Table 2), the parametric volume included voxels corresponding to atelectasy developing close to the tumor site. Although the change does not correspond to tumor growth or tumor regression, it was not considered that having it displayed in the parametric volume was a problem, especially given that it can be easily recognized as the result of atelectasy. The third case for which the tumor volume considered to have changed between the two scans was larger on the parametric volume than the difference between the two tumor volumes as measured from the two separate scans might be explained by partial volume effect (PVE).

4. DISCUSSION AND CONCLUSION

We have presented a parametric imaging approach for comparing successive PET scans in the context of patient monitoring. It was first found that accurate co-registration of two PET scans acquired several weeks apart was locally feasible by using the CT data acquired during the same imaging session as the PET data. We did not attempt to register the whole PET datasets but considered only the relevant slices given the tumor location, to facilitate the registration procedure. When several tumor sites were relevant, registration of the set of slices corresponding to each tumor was performed independently. Although we did not precisely assess the registration accuracy (work in progress), it was visually found sufficient to allow for a subsequent comparison of the two PET datasets at a voxel level.

The biparametric graphs obtained from the subtraction of the two PET volumes to be compared showed typical features, allowing for an easy crude recognition of patterns corresponding to noise only, non-tumor physiological changes, and tumor related changes (Figure 1). A precise analysis of these graphs using a Gaussian mixture model made it possible to precisely identify clusters corresponding to noise, non-tumor physiological changes and tumor-related changes. Focusing on tumor-related changes only, the parametric images makes it possible for the physician to immediately detect substantial changes in the tumor features (SUV and volumes), without any preliminary identification of the tumor regions (although the slices including the tumor have to be selected before the registration procedure). A 3D display of the parametric images showing the tumor change superimposed with the CT is obviously possible (Figure 2). Such representation might help identifying tumor region with heterogeneous response.

The quantitative analysis of the parametric images performed so far was extremely simple but was sufficient to check the consistency of the SUV and volume values affected by changes between the 2 scans derived from the parametric images with those measured by comparing the parameters measured in each of the 2 PET volumes. More detailed quantitative analysis of the parametric images will be developed, to account for partial volume effect affecting the parametric images.

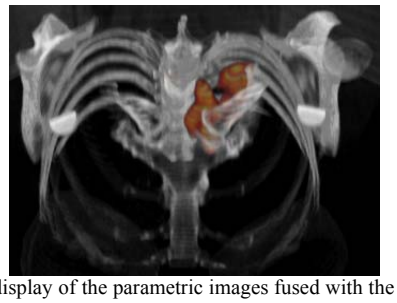

Fig. 3. 3D display of the parametric images fused with the initial CT.

The parametric imaging method has been successfully applied to 15 pairs of PET/CT scans in lung cancer patients. More evaluation is needed to test the robustness and the value of the approach in a broader range of applications. Tests on patients with lymphomas are currently under way.

6. REFERENCES

[1] G.J. Kelloff, et al, "Progress and Promise of FDG-PET Imaging for Cancer Patient Management and Oncologic Drug Development," *Clin Cancer Res*, vol. 11, pp. 2785-2808, 2005.

[2] N.G. Mikhaeel, "Use of FDG-PET to monitor response to chemotherapy and radiotherapy in patients with lymphomas," *Eur J Nucl Med Mol Imaging*, vol. 33, pp 22-26, 2006.

[3] JA.Thie, "Understanding the standardized uptake value, its methods, and implications for usage," *J Nucl Med*, vol. 45, pp 1431-1434, 2004.

[4] H. Young, "Measurement of clinical and subclinical tumour response using [18F]-fluorodeoxyglucose and positron emission tomography: review and 1999 EORTC recommendations," *Eur J Cancer*, vol. 35, pp 1773-1782, 1999.

[5] J. Hicks, "The role of PET in monitoring therapy," *Cancer Imaging*, vol. 5, pp 51-57, 2005.

[6] N.C. Krak, "Effects of ROI definition and reconstruction method on quantitative outcome and applicability in a response monitoring trial," *Eur J Nucl Med Mol Imaging*, vol. 32, pp 294-301, 2004.

[7] H.M. Hudson, et al, "Accelerated image reconstruction using ordered subsets of projection data," *IEEE Trans Med Imaging*, IEEE, vol. 13, pp 601-609, 1994.

[8] Z. Ouksili, et al, "Accurate PET-PET registration to assess lung tumor evolution,". *4th IEEE International Symposium on Biomedical Imaging*, pp 732-735, 2007.

[9] P. A. Freeborough, et al, "Accurate registration of serial 3D MR brain images and its application to visualizing change in neurodegenerative disorders," *J Comp Assist Tomogr*, vol. 20, pp. 1012–1022, 1996.

[10] R. P. Woods, et al, "Automated image registration: 1. General methods and intrasub- ject, intramodality validation," *J Comp Assist Tomogr*, vol. 22, pp. 139–152, 1998.

[11] M. Holden, et al, "Voxel similarity measures for 3d serial mr brain image registration," *IEEE Trans Med Imaging,* vol. 19, pp. 94–102, 2000.

[12] G. Celeux and G. Govaert. "Gaussian parsimonious clustering models". *Pattern Recognition,* vol. 28, pp. 781-793, 1995.

[13] C.Biernackia, et al, "Model-based cluster and discriminant analysis with the MIXMOD software," *Comput Statistics Data Anal,* vol. 51, pp 587-600, 2006.

[14] U. Nestle, et al, "Comparison of different methods for delineation of 18F-FDG PET-positive tissue for target volume definition in radiotherapy of patients with non-small cell lung cancer," *J Nucl Med*, vol. 46, pp 1342–1348, 2005.